Biophysical Chemistry 253 (2019) 106222

Contents lists available at ScienceDirect

Biophysical Chemistry

journal homepage: www.elsevier.com/locate/biophyschem

Density variations of TMAO solutions in the kilobar range: Experiments, PC-SAFT predictions, and molecular dynamics simulations

Michael Knierbein[a], Christoph Held[a], Christoph Hölzl[b], Dominik Horinek[b], Michael Paulus[c], Gabriele Sadowski[a], Christian Sternemann[c], Julia Nase[c,*]

[a] Technische Universität Dortmund, Laboratory of Thermodynamics, D-44221 Dortmund, Germany
[b] Institut für Physikalische und Theoretische Chemie, Universität Regensburg, 93040 Regensburg, Germany
[c] Technische Universität Dortmund, Fakultät Physik/DELTA, D-44221 Dortmund, Germany

HIGHLIGHTS

- We determined the density of pressurized TMAO solutions by experiments and theory.
- X-ray absorption is suitable to determine densities at pressure in the kbar range.
- PC-SAFT allows predicting density of aqueous TMAO solutions at high pressure.
- X-ray absorption, thermodynamic modeling, and MD simulations are in good agreement.
- TMAO decreases the compressibility, reflecting a locally stabilized water structure.

GRAPHICAL ABSTRACT

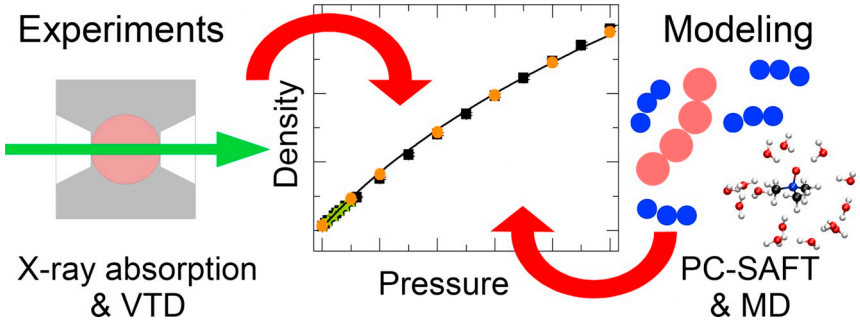

ARTICLE INFO

Keywords:
Density determination
TMAO solutions
High hydrostatic pressure
X-ray absorption measurements
PC-SAFT modeling
Molecular dynamics

ABSTRACT

We present measurements, molecular dynamics (MD) simulations, and predictions using Perturbed-Chain Statistical Associating Fluid Theory (PC-SAFT) of the density of aqueous solutions in a pressure range from 1 bar to 5000 bar, a pressure regime that is highly relevant for both biochemical applications and the fundamental understanding of solvation. The accurate determination of density data of pressurized solutions remains challenging. We determined relative density changes from the variations in X-ray absorption through the sample and developed a new water parameter set for PC-SAFT modeling that is appropriate for high pressure conditions in the kilobar regime. As a showcase, we studied trimethylamine *N*-oxide (TMAO) solutions and demonstrated that their compressibility decreases with the TMAO content. This result is linked to the stabilizing effect of TMAO on the local H-bond network of water. Experiments and calculations, which represent two independent methods, are in very good agreement and are in accordance with results of force field molecular dynamics simulations of the same systems.

1. Introduction

High pressure influences the thermodynamic properties of biochemical systems in a similar way to what is known for temperature, with the advantage of being a non-disruptive influence factor, which can readily be applied especially in the field of biochemistry or

* Corresponding author.
E-mail address: julia.nase@tu-dortmund.de (J. Nase).

https://doi.org/10.1016/j.bpc.2019.106222
Received 6 May 2019; Received in revised form 10 July 2019; Accepted 10 July 2019
Available online 12 July 2019

pharmaceutics. Notably, intermolecular bonds are not disrupted as long as the pressure is lower than approximately 20 kbar.

In the context of biochemical production processes, where enzymes are used to synthesize biochemical products, reaction conditions are limited to a narrow window regarding temperature, concentration, and pressure. These conditions determine the activity and stability of the enzyme [1–5]. For certain osmolytes, stabilizing and destabilizing effects on enzyme stability have been investigated [6–12]. It is also well known that enzymes denature at high temperatures [1–3]. In contrast, the application of high pressure counteracts these temperature denaturation effects to a certain extent [1–4,13–15]. Pressurization has even a positive effect on the activity of piezophile enzymes [1–4,13,14]. Consequently, knowledge about combined pressure and osmolyte effects is highly important. A well-studied osmolyte that can be used to counteract denaturation effects of enzymes is trimethylamine N-oxide (TMAO) [5,6,9–12,16–19]. It can be found in many organisms living at deep sea conditions and contributes to counteracting pressure effects. TMAO has been shown to influence the pressure-dependent interaction potential in lysozyme solutions [20,21]. Effects of TMAO on enzymes have been studied experimentally [5,10,13,14,22] and by simulations, especially MD simulations [7,12,23–25] at ambient pressure as well as at high pressure conditions. However, to tune and validate the applied MD models, data is needed about the compound's behavior under desired high pressure conditions. For this purpose, density data of aqueous solutions can be used. Pressure-counteracting effects of TMAO were also studied using statistical thermodynamics approaches, like the Kirkwood - Buff theory, a fluctuation solution theory where density data is of high importance (see e.g. [26]). The reliable analysis of THz spectroscopy data of fluids is likewise only possible if the density is known with high precision [27,28]. The knowledge of density data is further required to convert concentration scales such as molarity to mole fraction or molality. Despite the importance of density data of solutions at pressure, the availability is limited.

At ambient pressure, it is unproblematic to experimentally determine aqueous solution densities with high accuracy, but the task is challenging under high pressure conditions. A standard method is the determination of the longitudinal and transversal speeds of sound by applying Brillouin light scattering spectroscopy, from which thermodynamic quantities can be deduced, see for example [29–32]. This method can be applied in a wide temperature and pressure range. In order to determine densities in a very high pressure regime of up to 1.3 Mbar (130 GPa) in diamond anvil cells, the absorption of X-rays has been successfully used, see e.g. [33,34]. Commercial devices for laboratory density determination are available for pressures up to 500 bar, while for pressures in the kilobar range, commercially available density meters do not exist to our knowledge. Thus, it is advantageous to use thermodynamic models to predict desired properties under extreme conditions. Different approaches already exist to model the influence of high pressure and temperature on liquid densities. In first attempts, empirical correlations were used to simply describe the effects of pressure and temperature on density. Even though thermodynamic effects are not accounted for explicitly, this approach is still being used since it does not require complex models [35,36]. In contrast, thermodynamic models can be used to model pressure and temperature influences on liquid densities. Shock et al. used the Helgeson-Kirkham-Flowers equation of state to successfully model high-pressure and temperature effects on the density of aqueous solutions of gases and salts [37,38]. Further, the group of Pereira applied the Peng-Robinson equation of state to model the high-pressure density of gas and *n*-alkane mixtures [39]. Recently, Liu et al. compared different thermodynamic models regarding their performance to predict high-pressure and high-temperature effects on densities of different hydrocarbon systems [40]. Their work showed that Perturbed-Chain Statistical Associating Fluid Theory (PC-SAFT) [41] was the most suitable model for this purpose, leading to the lowest mean absolute percentage deviation.

In the current work, we show for the first time that X-ray absorption measurements yield precise results for pressurized solutions in the kilobar regime and in a experimental setup other than diamond anvil cells. The density of aqueous trimethylamine *N*-oxide solutions is investigated for pressures up to 5000 bar experimentally and theoretically. We determine relative density changes from X-ray absorption measurements, with a calibration to data obtained in a vibrating-tube density meter at 500 bar. Besides experimental density determination, the thermodynamic model PC-SAFT [41] was used to predict densities of aqueous TMAO solutions. The prediction results were evaluated in comparison to the experimentally determined density data. The two main results are the following. First, X-ray absorption is a relatively easy and reliable method to determine relative density changes from aqueous solutions in the kilobar range and second, PC-SAFT is a well-adapted modeling technique to predict thermodynamic variables in the high pressure regime with the newly established parameter set. Additionally, we performed predictive force field molecular dynamics simulations using a TMAO model that was adapted for high pressure conditions [25]. We found that the results of all methods are in excellent agreement.

2. Materials and methods

2.1. Sample preparation

TMAO solutions with $m = 0.522$ moles TMAO per kilogram pure water ($c = 0.5$ mol/L) or $m = 2.35$ moles TMAO per kilogram pure water ($c = 2$ mol/L) were prepared by weighing the appropriate amount of TMAO dihydrate and adding water (MilliQ, resistivity $R = 18.2$ MΩ cm) to the desired volume. TMAO hydrate was purchased from TCI and Merck with a purity of > 98 % and used without further treatment. The components were weighed in using a Sartorius laboratory balance with an accuracy of 0.0001 g. For absorption measurements, the liquids were degassed for 10 min directly before the experiments.

2.2. Absorption measurements

Lambert-Beer's law states that the intensity A_0 of radiation with energy E that passes the distance D in matter with the linear absorption coefficient $\mu(E)$ is attenuated following

$$A_1(D,E) = A_0 \mathrm{e}^{-\mu(E)D} \tag{1}$$

We are considering here X-rays with an energy that is far away from any absorption edges of the involved elements. The linear absorption coefficient $\mu(E)$ depends on the density of the material as

$$\mu(p,E) = \rho(p)\sigma(E) \ ,$$

where $\sigma(E)$ denotes the mass attenuation coefficient and $\rho(p)$ the homogeneous density. Thus, $\mu(E)$ depends on the pressure and the density can in principle be accessed via absorption measurements. It follows for the density that

$$\rho(p) = \ln\left(\frac{A_0}{A_1(p)}\right)\frac{1}{D\,\sigma(E)} \tag{2}$$

As it is difficult to directly detect the number of incident and transmitted photons with the required accuracy, we determine relative density changes instead of absolute values. In our experimental setup, the electric currents in ionization chambers before (I_0) and after (I_1) the sample are measured. They are both linked to the intensities $A_0 = c_0 I_0$ and $A_1 = c_1 I_1$. The amplification factor ratio c_0/c_1 of both ionization chambers needs to be known for further data analysis and can be extracted from a water reference, as detailed later. Relative density changes can then be determined within a pressure series, and the data is calibrated to a known density at low pressure, measured by an independent method as the vibrating-tube density meter.

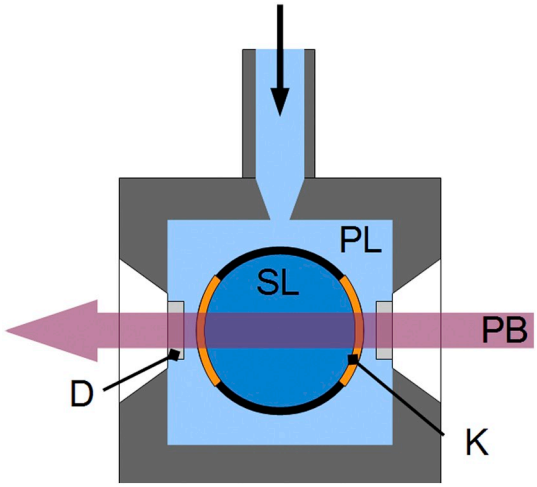

Fig. 1. Beam path through the high pressure cell. PL = pressure transmitting liquid; SL = sample liquid; PB = photon beam; K = Kapton windows; D = diamond disks.

Experiments were performed in a custom-build high pressure cell that can sustain pressures up to 5000 bar. [42]. This cell is designed for X-ray reflectivity measurements, but is well-adapted for absorption experiments if the cell is used in a transmission configuration. The cell consists of an outer shell that guarantees the pressure stability. Inside the cell, a small inner cell, which contains the sample liquid, is embedded. The sample volume of approximately 0.75 mL is separated from the pressure-transmitting liquid (water) by two Kapton windows and a flexible membrane. The latter is transmitting the pressure to the sample volume, ensuring thus that the Kapton windows in beam direction are only deformed slightly when pressure is applied. The cell is sealed towards the outside by two diamond disks with a diameter of 6 mm and a thickness of 1 mm. Absorption experiments were performed at beamline BL8 of DELTA at an incident energy of the synchrotron radiation between 16.81 keV to 16.91 keV [43]. The beam size was approximately 1 mm × 1 mm. The ionization chambers before and after the sample were filled with Argon and Xenon, respectively. The sample temperature was set to 298 K and 300 K, and the pressure stability was better than 1 %.

In the experimental set-up, see the sketch in Fig. 1, the X-ray beam passes two diamond windows (D), two Kapton windows (K), and the sample (SL) with length d_s. In addition, there are two thin layers, each with a thickness of $d_w/2$, between sample and diamond windows that are filled with the pressure transmitting medium (PL), which is water. This small water layer adds additional absorption contributions. In the following, we consider d_s and d_w to be constant with pressure. This assumption is valid since the small flexible membrane is compensating for volume changes inside the cell as the pressure is increased, and will be discussed later in more detail. As per construction of the cell, d_s = 9800 μm and $d_w = 2 \cdot 100$ μm.

$I_1(E,p)$ and I_0 were measured over the entire energy range from 16.81 keV to 16.91 keV with a step size of 0.001 keV. Since this energy range is very small and far from any absorption edges of the elements in the sample, the quantity $\ln \frac{I_0}{I_1}$ can be approximated with a linear function. The quantity $M(p)$ is defined as $M(p) = \sum \ln \frac{I_0}{I_1}$ of the fitted data over this energy range at a given pressure. Likewise, $\mu(E)$ depends linearly on the energy in the considered energy range and $\bar{\mu}_{w/s}(p)$ is the mean linear absorption coefficient of water or sample.

If the sample volume is filled with water, Eq. (1) reads

$$A_1(p) = A_0 e^{-\mu_w(E,\ p)(d_w + d_s)} \tag{3}$$

and thus

$$\ln \frac{I_0}{I_1} + \ln \frac{c_0}{c_1} = \mu_w(E,\ p)(d_w + d_s) \tag{4}$$

With $c = \ln \frac{c_0}{c_1}$, we can deduce

$$M(p) + c = \bar{\mu}_w(p)(d_w + d_s) \tag{5}$$

Changes in the quantity $M(p)$ relative to a reference pressure p_0 can then be expressed as

$$\frac{M(p) + c}{M(p_0) + c} = \frac{\bar{\mu}_w(p)}{\bar{\mu}_w(p_0)} \tag{6}$$

It follows with $\mu = \rho\ \sigma$ for the water reference measurement that

$$\frac{\rho(p)}{\rho(p_0)} = \frac{M(p) + c}{M(p_0) + c} \tag{7}$$

The parameter c is determined by adjusting the right side of Eq. (7) with c being the only fit parameter by a least mean square algorithm, so that the sum of the squared differences between the experimental data $R_{Exp} = \frac{M(p)+c}{M(p_0)+c}$ and the literature data $R_{NIST} = \rho(p)/\rho(p_0)$ as available from reference [44] is minimal:

$$\sum |R_{Exp} - R_{NIST}|^2 \stackrel{!}{=} 0 \tag{8}$$

Fig. 2 shows results of the fitting procedure of two independent water reference measurements. The experimental data (blue squares and red stars) fall perfectly onto the data from NIST (black line) after fitting c. The residuum, that is, the sum of the squared differences between reference data and experimental data normalized to the number of data points, is on the order of 10^{-8} to 10^{-7}. The lower panels in the figure (red and blue crosses) show the difference between experimental and NIST data for each data point.

When the cell is filled with the sample liquid, there are contributions from the sample and the thin pressure transmitting water layer, resulting in the equation

$$\frac{M(p) + c}{M(p_0) + c} = \frac{\bar{\mu}_s(p)d_s + \bar{\mu}_w(p)d_w}{\bar{\mu}_s(p_0)d_s + \bar{\mu}_w(p_0)d_w} \tag{9}$$

with μ_s indicating the sample material. It follows

$$\bar{\mu}_s(p) = \frac{M(p) + c}{M(p_0) + c}\left[\frac{\bar{\mu}_s(p_0)d_s + \bar{\mu}_w(p_0)d_w}{d_s}\right] - \frac{\bar{\mu}_w(p)d_w}{d_s} \tag{10}$$

In this equation, $M(p)$ and $M(p_0)$ are measured in the experiment, c is determined from the water reference as described above, $\bar{\mu}_s(p_0)$ is calculated from the reference density of the sample measured in the vibrating-tube density meter and the mass attenuation coefficient σ in the given energy range, which can be obtained from data bases as XCOM [45]. $\bar{\mu}_w(p)$ is likewise calculated from the mass attenuation coefficient and the pressure-dependent density of water [44]. Thus, all variables in Eq. (10) are either known or can be measured, and consequently, $\bar{\mu}_s(p)$ can be calculated. The desired sample density as a function of pressure follows from a simple division by the mass absorption coefficient as

$$\rho_s(p) = \frac{\bar{\mu}_s(p)}{\sigma_s}$$

The experimental absorption data that are presented in the following were obtained in this way. The mean values and error bars of ρ were determined by analyzing several independent pressure series.

In the analysis as described above, we assume that the absorbing length of the sample d_s and the thin water layer d_w are constant with pressure. To evaluate possible effects of a varying thickness d_w, we repeated the analysis of a TMAO solution with m = 2.35 mol/kg for d_w = 0 μm, d_w = 200 μm, and d_w = 500 μm, corresponding to d_s = 10000 μm, d_s = 9800 μm, and d_s = 9500 μm. Fig. 3 displays for all three values of d_w the difference in the resulting density as compared to d_w = 200 μm, which is the nominal value as per construction of the cell.

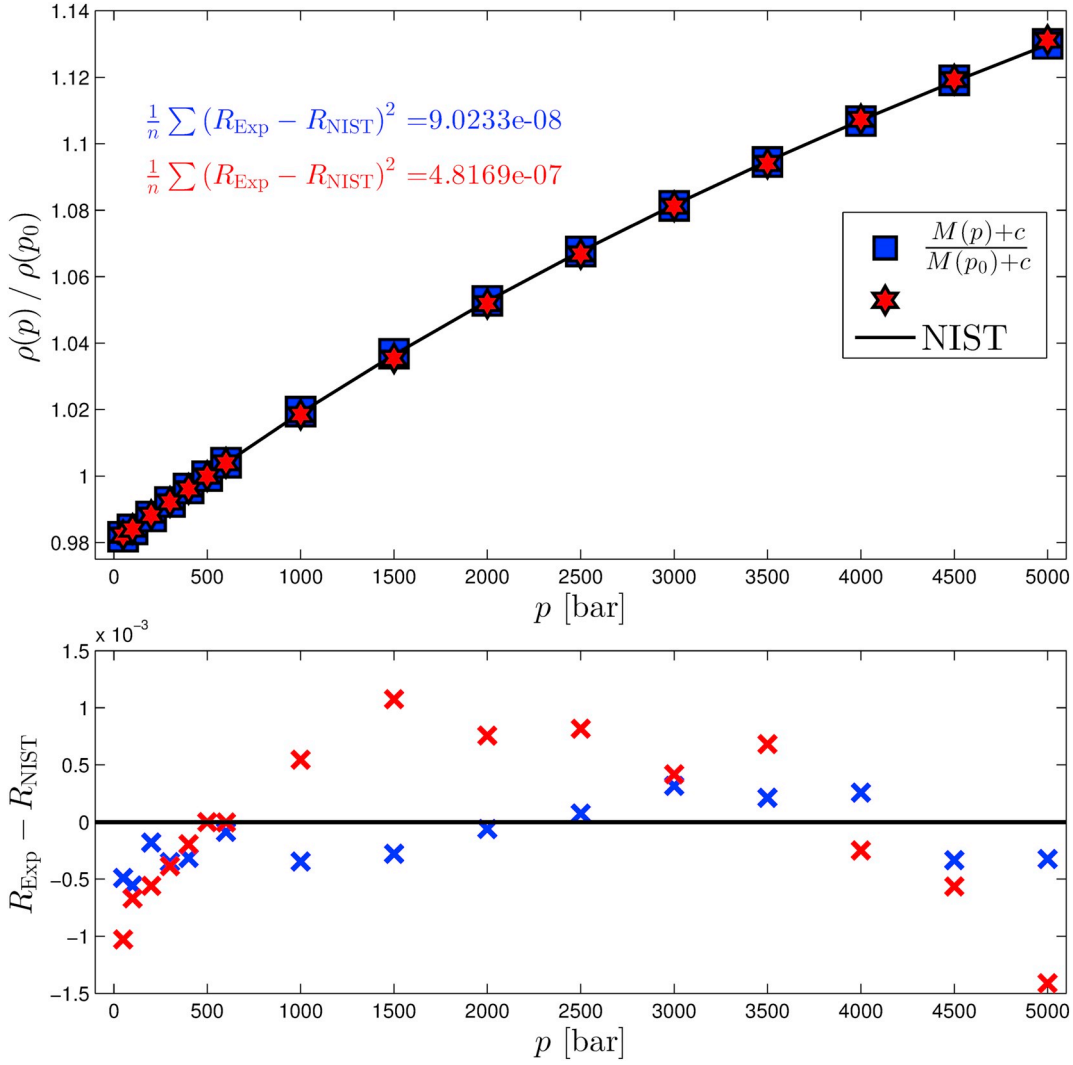

Fig. 2. Determination of the constant c from two independent reference measurements on water samples (blue squares and red stars). The lower panel shows the difference between experimental and NIST data for each data point of the two samples. (For interpretation of the references to colour in this figure legend, the reader is referred to the web version of this article.)

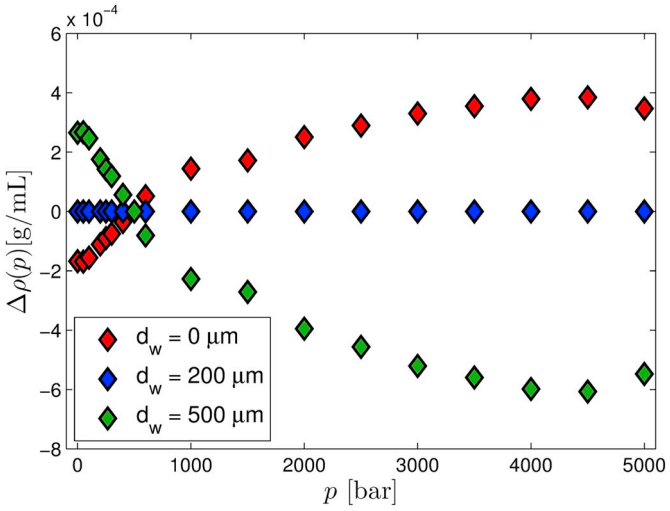

Fig. 3. Influence of the assumed thickness d_w on the resulting density values.

We can conclude that the maximum discrepancy between d_w = 0 µm and d_w = 500 µm appears at p = 4500 bar, with a variation of below 0.001 g/mL.

2.3. Vibrating-tube density meter

As discussed before, the density of the sample must be known at a given reference pressure (here, p_0 = 500 bar) for a reliable analysis of the absorption measurements. The reference density measurements were performed using an Anton Paar vibrating-tube density meter DMA 4200 M. The method is based on a pulsed excitation and allows highly precise density measurements with an accuracy of 0.2 kg/m^3 at controlled temperature. The accuracy of the measured temperature is 0.03 K and the manufacturer's specified reproducibility is 0.1 kg/m^3. The instrument was calibrated using water and *n*-heptane. The measurement method was validated by comparing the measured density of a 1 mol/L aqueous sodium chloride solution to literature data [46], which resulted in an average relative deviation (ARD) of 0.028 % and an average absolute deviation (AAD) of 0.29 kg/m^3. Density measurements were performed at a temperature of 298 K and 300 K, respectively, for TMAO solutions with a molality of 0.522, 1.082, or 2.350 moles TMAO per kg pure water, being equivalent to a molarity of 0.5, 1, or 2 moles TMAO per liter solution. The density was measured in steps of 100 bar to a maximum pressure of 500 bar, the data is given in Tables 1 to 5. All measurements were performed at least twice with a maximum deviation of 0.1 kg/m^3, being equal to a reproducibility of 0.01 %. Fig. 4 shows the experimentally determined densities of aqueous TMAO solutions at 298.15 K in comparison to literature data [47]. Very

Table 1
PC-SAFT pure-component parameters for HP-water and TMAO. HP-water from this work, TMAO from [53]. The binary interaction parameter between HP-water and TMAO is $k_{ij} = -0.15 - 0.005417$ T.

	m_i^{seg}[−]	σ_i[Å]	u_i/k_B[K]	ε^{AiBi}/k_B[K]	κ^{AiBi}[−]	Association scheme
HP-water	1.442	2.612	113.47	2171.8	0.070	2:2
TMAO	8.928	2.248	245.44	0	0.070	1:1

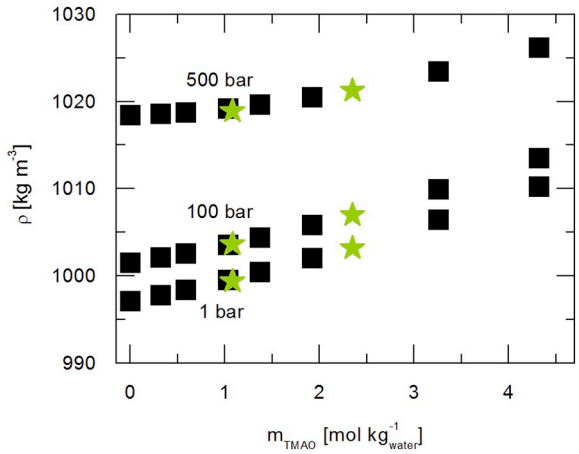

Fig. 4. Density of aqueous TMAO solutions plotted against TMAO molality at 298.15 K. Green stars: experimental results from the vibrating-tube density meter, squares: literature data [47]. (For interpretation of the references to colour in this figure legend, the reader is referred to the web version of this article.)

good agreement with literature was obtained at pressures between 1 bar and 500 bar.

2.4. Molecular dynamics simulations

In molecular dynamics simulations, the reliability of classical force fields is highest for the conditions at which they were optimized. Concerning pressure variations in water, high pressures lead to an increased polarization of solutes. This can be accounted for by pressure-dependent atomic partial charges. We have previously optimized a nonpolarizable force field for TMAO that accounts for the increased polarization of TMAO in water at elevated pressures by scaling the partial charges [25]. Here, we use this force field in combination with the TIP4P/2005 water model [48] to simulate a 2.35 mol/kg TMAO solution at six pressures from 1 bar to 5 kbar in order to calculate the solution densities. Computational details and system compositions are identical to those in ref. [25]. We also show density data of the 0.522 mol/kg TMAO system, which was taken from the same reference. The rational activity coefficients in the molality scale (γ^*) were calculated via Kirkwood-Buff theory [49] using the method by Cortes-Huerto et al. [50]. G_{ij} denote the Kirkwood-Buff integrals, and the indices T and W refer to TMAO and water respectively.

$$-\left(\frac{\partial \ln \gamma_T^*}{\partial \ln m_T}\right)_{p,T} = \frac{c_T + c_T c_W (G_{TT} + G_{WW} - 2G_{TW})}{c_T + c_W + c_T c_W (G_{TT} + G_{WW} - 2G_{TW})} \quad (11)$$

2.5. PC-SAFT modeling

The thermodynamic model PC-SAFT [41] was used to predict the density of aqueous TMAO solutions of defined TMAO molality at a pressure range of 1 bar to 5000 bar. Within PC-SAFT, each molecule is described as a chain of spherical segments, each of them defined by the segment diameter and the number of segments. The attractive interactions between the molecules are characterized by dispersion and association forces. Based on these model contributions, PC-SAFT calculates the residual Helmholtz free energy A^{res} in a mixture. A^{res} is calculated as the sum of the hard chain A^{HC}, dispersion A^{disp}, and association A^{assoc} Helmholtz energy contributions to the residual Helmholtz free energy. The number of association sites as well as the corresponding association energy and the association volume are required for A^{assoc}. PC-SAFT is suited to predict pressure effects since it explicitly accounts for pressure disturbances [41]. Furthermore, PC-SAFT has proven to predict fluid densities very accurately in scientific literature [8,51–53]. PC-SAFT predictions were calculated for aqueous solutions at defined conditions (pressure p, temperature T, and composition x_i). The PC-SAFT parameters for all components used in this work are given in Table 1. Induced association was accounted for between water and TMAO according to Kleiner et al. [54]. In this work, the solute's (TMAO) PC-SAFT parameters were taken from literature [53] and only the binary interaction parameter k_{ij} between water and TMAO was fitted to osmotic coefficient and solution density data. Consequently, only one parameter was fitted to simultaneously describe numerous mixture data. Please note that in the following, 'HP-water' denotes water that is modeled in the high-pressure range with a new PC-SAFT parameter set.

In order to achieve highly accurate predictions for the density of aqueous solutions, it is crucial to model the density of liquid water itself at high-pressure conditions with satisfying accuracy. Due to its characteristic and often anomalous properties, water is challenging to model using PC-SAFT or comparable models. Thus, many pure-component parameter sets for water exist in scientific literature [51,55–59]. However, all of these proposed parameter sets fail to predict the density of water with satisfying accuracy over a wide pressure scale up to the kilobar range. The commonly used parameter set for water in biochemical applications was developed by Cameretti et al. [51]. It is especially suitable to model the behavior of pure water and aqueous mixtures at conditions common for biochemical processes, i.e. for $p < 10$ bar and $T <= 373$ K. However, at high pressure conditions, this parameter set fails to predict the liquid density (see the dashed line in Fig. 5). While the density is modeled at 1 bar with an accuracy of 0.03 %, the deviation between predicted and experimental density at 9500 bar is 8.5 %. For the pressure range from 1 bar to 9500 bar, the liquid density is predicted with an unsatisfying AAD of 54.25 kg/m^3 (ARD = 4.7 %).

As a consequence, a new parameter set for water was developed in this work that is especially suitable to model high-pressure density data. The new PC-SAFT parameters for HP-water that were fitted to vapor pressure data and density data are given in Table 1. PC-SAFT modeling results for the water density from 1 bar to 10,000 bar are illustrated in

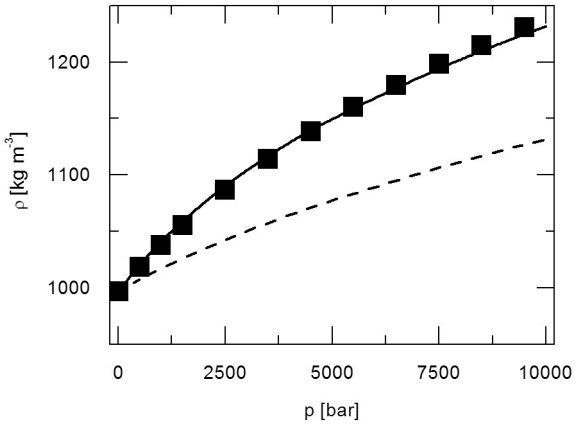

Fig. 5. Density of pure water in kg/m^3 plotted against pressure in bar at 298.15 K. Squares: literature data [60], dashed line: PC-SAFT modeling results using state-of-the-art water parameters from Cameretti and Sadowski [51], solid line: PC-SAFT modeling results using newly determined PC-SAFT parameters for HP-water [this work from Table 1].

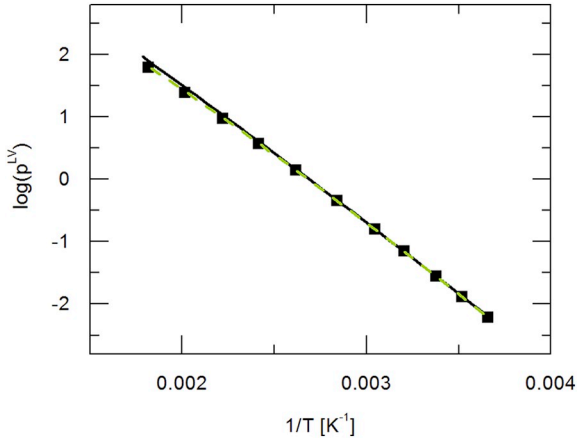

Fig. 6. Logarithm of the vapor pressure (in bar) of water plotted against the inverse temperature (in K). Squares: literature data [60], dashed line: PC-SAFT modeling results using state-of-the-art water parameters from Cameretti and Sadowski [51], solid line: PC-SAFT modeling results using newly determined PC-SAFT parameters for HP-water [this work using parameters from Table 1].

Fig. 5 (solid line). Clearly, the new PC-SAFT parameters for HP-water allow modeling the density very well with a maximum deviation of 0.5 % at 9500 bar. For the pressure range from 1 bar to 9500 bar, the density can be modeled accurately with an AAD of 2.71 kg/m^3 and an ARD of 0.24%.

In Fig. 6, the logarithm of the vapor pressure from PC-SAFT modeling is plotted against the inverse temperature. The results show that both parameter sets are well suited to model the vapor pressure of pure water with high accuracy. In a temperature range from 275 K to 560 K, the state-of-the-art water parameters lead to an AAD of 0.4 bar, while the new HP-water parameters result in an AAD of 2.0 bar.

After the verification that the new parameter set works reliably for pure water, the next step was the modeling of aqueous TMAO solutions. For TMAO, the pure-component parameters published by Held et al. were used [53]. This parameter set was fitted to solution density data and osmotic coefficients of TMAO aqueous solution. Due to new HP-water parameters determined in this work, the binary interaction parameter k_{ij} between HP-water and TMAO was fitted to density data and experimental osmotic coefficients. In a first modeling step of this work, the density of aqueous TMAO solutions was modeled at 298.15 K and 1 bar and evaluated using literature data from Makarov et al. [47], see Fig. 7. The modeling results have a maximum deviation of 0.034 % at a molality of 0.4018 mol/kg. For the considered concentration range, the AAD is 0.139 kg/m^3 and the ARD is 0.014 %.

Both the modeled aqueous density and the osmotic coefficients of TMAO solutions show that the HP-water parameters are very well suited to model binary volumetric and energetic properties of aqueous TMAO solutions at ambient pressure. Given these results, we modeled in a final step volumetric properties of aqueous TMAO solutions at high-pressure conditions. The densities of 0.522 mol/kg and 2.35 mol/kg TMAO solutions were predicted at 300.15 K and 298.15 K, respectively, for pressures up to 5000 bar.

3. Results and discussion

Figs. 8 and 9 display the overall combined results of our experimental and simulation work. The PC-SAFT modeling, molecular dynamics simulations, and the data from X-ray absorption measurements agree very well concerning the pressure influence on the density of the aqueous TMAO solutions for all concentrations under investigation. Comparing the experimentally determined densities up to 500 bar from the vibrating-tube density meter with the corresponding PC-SAFT predicted densities of aqueous TMAO solutions yields a maximum ARD of 0.18 %. Evaluating the

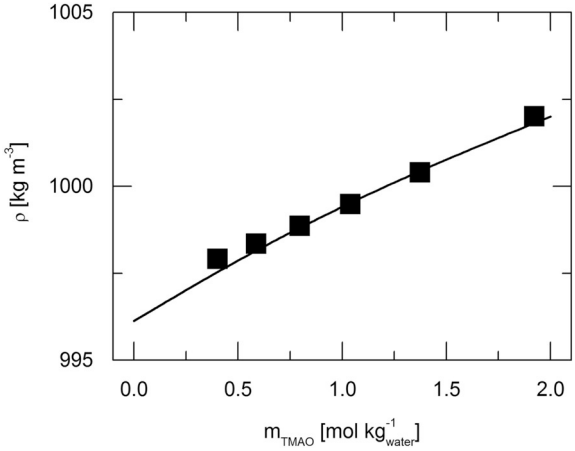

Fig. 7. Density of aqueous TMAO solutions at 298.15 K and 1 bar plotted against molality of TMAO. Symbols: literature data [47], line: PC-SAFT modeling results.

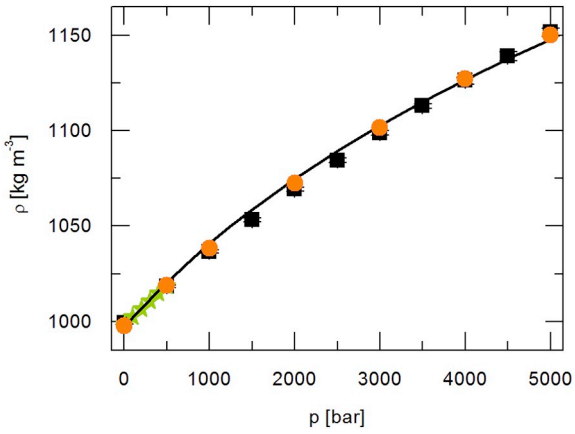

Fig. 8. Density of 0.522 mol/kg aqueous TMAO solutions plotted against pressure at 300.15 K. Green stars: experimental results from the vibrating-tube density meter, black squares: experimental results from the X-ray absorption measurements, orange circles: MD simulations, line: PC-SAFT modeling results using parameters from Table 1. (For interpretation of the references to colour in this figure legend, the reader is referred to the web version of this article.)

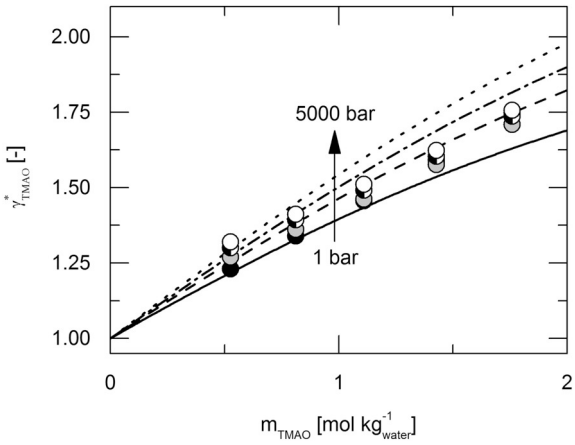

Fig. 9. Density of 2.35 mol/kg aqueous TMAO solutions plotted against pressure at 298.15 K. Stars: experimental results from the vibrating-tube density meter, black squares: experimental results from the X-ray absorption measurements, orange circles: MD simulations, line: PC SAFT modeling results using parameters from Table 1.

predicted densities for pressures up to 5000 bar in comparison to the experimentally determined densities from X-ray absorption yields a maximum ARD of 0.31 %. It is important to note that the X-ray absorption technique and the PC-SAFT modeling are independent of each other. The absorption technique has as only input the TMAO density at 500 bar and literature data for water, PC-SAFT requires data for the properties of the pure components at ambient pressure. In that light, we show clearly that we present two independent approaches that are well suited to determine and predict high pressure and concentration effects on the density of aqueous TMAO solutions over a very wide pressure range. In principle, the X-ray absorption technique is well-suited to determine relative density changes in any other solution with known reference density and known composition.

The experimental results from the vibrating-tube density meter show, in agreement with literature, that the concentration of TMAO has a significant influence on the solutions density at 1 bar. However, the density difference between water and aqueous TMAO solutions depends non-linearly on pressure. Indeed, we found in experiments, simulations and calculations under high-pressure conditions that the 2.35 mol/kg TMAO solution has a lower density than the 0.522 mol/kg TMAO solution for pressures above 2500 bar. The density of the aqueous 2.35 mol/kg solution is even lower than the density of pure water in the same pressure range. At 5000 bar and 298 K, the density of the 2.35 mol/kg TMAO solution is 1147.3 kg/m^3 in absorption experiments and 1143.1 kg/m^3 in PC-SAFT calculations, while the density of water is 1149.4 kg/m^3. We observed the same trend in molecular dynamics simulations, where the density of 2.35 mol/kg TMAO is 1144.8 kg/m^3, and the water density is 1153.4 kg/m^3. These observations are equivalent to the fact that aqueous TMAO solutions become less compressible the more TMAO is added, leading to a less pressure-responsive density of the liquids.

This behavior can be explained by solute/solute interactions between two TMAO molecules in aqueous solution. The increase in pressure results in weaker solute/solute interactions, while strengthening the solute's hydration [47]. Strengthening of the local water structure around TMAO was likewise found previously in experiments employing X-ray Raman scattering spectroscopy [61] and X-ray Compton scattering [62]. Further, the rational activity coefficient of the solution allows quantifying the effects of pressure on molecular interactions. As already applied by Baz et al. [63] the rational activity coefficient $\gamma_{TMAO}^{\star}$ is a measure of the change in solvation Gibbs energy of the solute in solution. Both, MD simulation and PC-SAFT modeling underline that higher pressure results in increased rational activity coefficients (see Fig. 10) and consequently in larger solvation Gibbs energies. The fact that the rational activity coefficient increases with increasing pressure might be caused by a higher density of water in the hydration shell of the TMAO molecules or by increased repulsive interactions between the TMAO molecules. Both effects would ultimately result in lower compressibility. MD simulations of Imoto et al. [24] gave further insight into molecular interactions between TMAO and water as well as between water molecules at high pressure conditions. They found that the application of p = 10 kbar on aqueous TMAO solutions has a rather complex effect on molecular interactions, which is distinctively different from the pressure response of pure water. While the hydrophilic oxygen site of TMAO has threefold H-bonding in their simulations at atmospheric pressure conditions, the probability of fourfold H-bonding rises at high pressure conditions from 10% to 40%. Contrary to that, the effect of high pressure on pure water was found to be simpler, but stronger in reference [24]: Each water molecule is surrounded by a hydrogen-bonded network of other water molecules, with four water molecules arranged in a tetrahedral structure with large voids in between. Under high pressure conditions, two more water molecules are squeezed into the voids of this tetrahedral arrangement, leading to a changed distribution of water molecules in this hydration shell. In total, the coordination number is significantly increased due to the intruding water molecules. The hydrogen bond network of TMAO is locally enhanced, and the solvation shell is therefore less affected by high pressure compared to water. For TMAO, not only the first hydration shell, but also the second shell is structurally robust against compression [24]. Consequently, we might conclude that the enhanced robustness of the water hydration shell structure in presence of TMAO molecules, which was observed by several authors in simulations and experiments, is linked to a decreased compressibility of TMAO solutions as compared to pure water. These results thus explain our findings from experiments, thermodynamic modeling, and MD simulations.

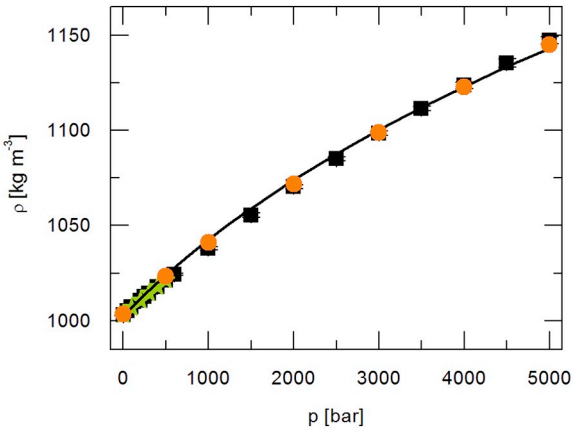

Fig. 10. Rational activity coefficient of TMAO in aqueous solution at 298 K and pressures from 1 bar to 5000 bar plotted against the molality of TMAO. Symbols: MD simulation results (black: 1 bar, grey: 1000 bar, black-white: 2000 bar, white: 5000 bar), lines: PC-SAFT modeling results using parameters from Table 1 (full: 1 bar, dashed: 1000 bar, dashed-dotted: 2000 bar, dotted: 5000 bar).

4. Conclusion

Thermodynamic properties of aqueous TMAO solutions were investigated in this work, notably the density of aqueous TMAO solutions under high pressure conditions both experimentally and theoretically. We determined new high pressure density data experimentally, in MD simulations and PC-SAFT predictions for pressures up to 5000 bar. At atmospheric pressure, PC-SAFT successfully modeled both energetic and volumetric data of TMAO solutions at different concentrations. Likewise, at high pressure conditions, PC-SAFT was able to predict density data for aqueous TMAO solutions with high accuracy. The modeling is in very good agreement with measurements of relative density changes from X-ray absorption experiments. Our finding that the compressibility of TMAO solutions decreases with the added amount of TMAO can be explained by results from MD simulations and experiments, where it was confirmed that the robustness of the water H-bond network is locally enhanced around TMAO molecules. Besides that, the main results of our study are the following. First, X-ray absorption in combination with our high pressure environment is a suitable method to determine relative density changes from aqueous solutions in the kilobar regime and second, PC-SAFT is a well-adapted modeling technique to predict thermodynamic properties in the high pressure regime with the newly established pure-component parameter set for water. Both approaches yield density values that are in quantitative agreement with MD simulations using a highly reliable force field.

The authors declare no competing interests.

Acknowledgement

We acknowledge the Deutsche Forschungsgemeinschaft (DFG) for funding in the framework of the Research Group FOR1979. We acknowledge Ralph Wagner for help with the experiments at beamline 8, and the DELTA crew for providing synchrotron radiation. We thank Jennifer Bolle, Mirko Elbers, Marc Moron, Mike Moron, Paul Salmen, Göran Surmeier, and Shaohan Zhu (all Technische Universität Dortmund) for supporting the absorption experiments.

Appendix

Table 2
Density of aqueous 0.522 mol/kg TMAO solutions at 300.15 K and at pressures from 1 bar to 500 bar determined using the vibrating-tube density meter.

p[bar]	1	100	200	300	400	500
ρ[kg/m^3]	998.37	1002.52	1006.61	1010.68	1014.67	1018.51

Table 3
Density of aqueous 1.082 mol/kg (1 mol/L) TMAO solutions at 298.15 K and at pressures from 1 bar to 500 bar determined using the vibrating-tube density meter.

p[bar]	1	100	200	300	400	500
ρ[kg/m^3]	999.38	1003.65	1007.91	1011.59	1015.37	1018.89

Table 4
Density of aqueous 2.35 mol/kg (2 mol/L) TMAO solutions at 298.15 K and at pressures from 1 bar to 500 bar determined using the vibrating-tube density meter.

p[bar]	1	100	200	300	400	500
ρ[kg/m^3]	1003.16	1007.01	1010.81	1014.33	1017.94	1021.23

Table 5
PC-SAFT predictions of aqueous 0.522 mol/kg (0.5 mol/L) TMAO solutions at 300.15 K and at pressures from 1 bar to 5000 bar.

p[bar]	1	100	200	300	400	500
ρ[kg/m^3]	996.96	1001.97	1006.85	1011.57	1016.13	1020.55
p[bar]	750	1000	1250	1500	2000	2500
ρ[kg/m^3]	1031.05	1040.86	1050.06	1058.74	1074.79	1089.38
p[bar]	3000	3500	4000	4500	5000	
ρ[kg/m^3]	1102.79	1115.21	1126.79	1137.66	1147.90	

Table 6
PC-SAFT predictions of aqueous 1.082 mol/kg (1 mol/L) TMAO solutions at 298.15 K and at pressures from 1 bar to 5000 bar.

p[bar]	1	100	200	300	400	500
ρ[kg/m^3]	999.67	1004.48	1009.18	1013.72	1018.12	1022.39
p[bar]	750	1000	1250	1500	2000	2500
ρ[kg/m^3]	1032.54	1042.04	1050.97	1059.41	1075.03	1089.27
p[bar]	3000	3500	4000	4500	5000	
ρ[kg/m^3]	1102.37	1114.53	1125.89	1136.55	1146.61	

Table 7
PC-SAFT predictions of aqueous 2.35 mol/kg (2 mol/L) TMAO solutions at 298.15 K and at pressures from 1 bar to 5000 bar.

p[bar]	1	00	200	300	400	500
ρ[kg/m^3]	1002.79	1007.28	1011.68	1015.94	1020.08	1024.09
p[bar]	750	1000	1250	1500	2000	2500
ρ[kg/m^3]	1033.68	1042.67	1051.15	1059.19	1074.11	1087.76
p[bar]	3000	3500	4000	4500	5000	
ρ[kg/m^3]	1100.36	1112.08	1123.05	1133.38	1143.13	

Table 8
Density of a 0.522 mol/kg (0.5 mol/L) TMAO solution at 300 K from X-ray absorption measurements.

p[bar]	50	500	1000	1500	2000	2500
ρ[kg/m^3]	999.2	1018.5	1036.6	1053.2	1069.2	1084.4
p[bar]	3000	3500	4000	4500	5000	
ρ[kg/m^3]	1098.7	1112.9	1126.2	1138.9	1151.6	

Table 9
Density of a 2.35 mol/kg (2 mol/L) TMAO solution at 298 K from X-ray absorption measurements.

p[bar]	50	100	200	300	400	500
ρ[kg/m^3]	1005.2	1007.1	1010.7	1014.3	1017.7	1021.2
p[bar]	600	1000	1500	2000	2500	3000
ρ[kg/m^3]	1024.3	1038.0	1055.3	1070.4	1084.9	1098.5
p[bar]	3500	4000	4500	5000		
ρ[kg/m^3]	1111.4	1123.6	1135.4	1147.3		

Table 10
Density of MD simulations of 0.522 mol/kg (0.5 mol/L) TMAO at 300 K from ref. [25].

p[bar]	1	500	1000	2000	3000
ρ[kg/m^3]	997.568	1018.96	1038.29	1072.42	1101.63
p[bar]	4000	5000			
ρ[kg/m^3]	1127.17	1150.08			

Table 11
Density of MD simulations of 2.35 mol/kg (2 mol/L) TMAO at 298 K.

p[bar]	1	500	1000	2000	3000
ρ[kg/m^3]	1003.59	1023.22	1040.94	1071.84	1098.99
p[bar]	4000	5000			
ρ[kg/m^3]	1122.75	1144.8			

Appendix A. Supplementary data

Supplementary data to this article can be found online at https://doi.org/10.1016/j.bpc.2019.106222.

References

[1] S.A. Hawley, Reversible pressure-temperature denaturation of chymotrypsinogen, Biochemistry vol. 10, (13) (1971) 2436–2442.
[2] L. Smeller, Pressure-temperature phase diagrams of biomolecules, Biochimica et Biophysica Acta (BBA)-protein Structure and Molecular Enzymology, vol. 1595, 2002, pp. 11–29 1-2.
[3] R. Winter, D. Lopes, S. Grudzielanek, K. Vogtt, Towards an understanding of the temperature/pressure configurational and free-energy landscape of biomolecules, J. Non-Equilibr. Thermodynam. 21 (2007) 41–97 1, S.
[4] M.J. Eisenmenger, J.I. Reyes-De-Corcuera, High pressure enhancement of enzymes: a review, Enzym. Microb. Technol. 45 (5) (2009) 331–347.
[5] A. Kumar, P. Venkatesu, Overview of the stability of alpha-chymotrypsin in different solvent media, Chem. Rev. 112 (7) (2012) 4283–4307.
[6] I. Baskakov, A. Wang, D.W. Bolen, Trimethylamine-N-oxide counteracts urea effects on rabbit muscle lactate dehydrogenase function: a test of the counteraction hypothesis, Biophys. J. 74 (5) (1998) 2666–2673.
[7] D.R. Canchi, P. Jayasimha, D.C. Rau, G.I. Makhatadze, A.E. Garcia, Molecular mechanism for the preferential exclusion of TMAO from protein surfaces, J. Phys. Chem. B 116 (40) (2012) 12095.
[8] C. Held, T. Neuhaus, G. Sadowski, Compatible solutes: thermodynamic properties and biological impact of ectoines and prolines, Biophys. Chem. 152 (1–3) (2010) 28–39.
[9] T.-Y. Lin, S.N. Timasheff, Why do some organisms use a urea-methylamine mixture as osmolyte? Thermodynamic compensation of urea and trimethylamine N-oxide interactions with protein, Biochemistry 33 (42) (1994) 12695–12701.
[10] J. Ma, I.M. Pazos, F. Gai, Microscopic insights into the protein-stabilizing effect of trimethylamine N-oxide (TMAO), Proc. Natl. Acad. Sci. U. S. A. 111 (23) (2014) 8476–8481.
[11] T. Mashino, I. Fridovich, Effects of urea and trimethylamine-N-oxide on enzyme activity and stability, Arch. Biochem. Biophys. 258 (2) (1987) 356–360.
[12] Q. Zou, B.J. Bennion, V. Daggett, K.P. Murphy, The molecular mechanism of stabilization of proteins by TMAO and its ability to counteract the effects of urea, J. Am. Chem. Soc. 124 (7) (2002) 1192–1202.
[13] T.Q. Luong, R. Winter, Combined pressure and cosolvent effects on enzyme activity-a high-pressure stopped-flow kinetic study on α-chymotrypsin, Phys. Chem. Chem. Phys. 17 (35) (2015) 23273–23278.
[14] M.W. Jaworek, V. Schuabb, R. Winter, The effects of glycine, TMAO and osmolyte mixtures on the pressure dependent enzymatic activity of α-chymotrypsin, Phys. Chem. Chem. Phys. 20 (3) (2018) 1347–1354.
[15] P.V. Iyer, L. Ananthanarayan, Enzyme stability and stabilization-aqueous and non-aqueous environment, Process Biochem. 42 (10) (2008) 1019–1032.
[16] K. G'Oller, E.A. Galinski, Protection of a model enzyme (lactate dehydrogenase) against heat, urea and freeze-thaw treatment by compatible solute additives, J. Mol. Catal. B Enzym. 7 (1-4) (1999) 37–45.
[17] T. Arakawa, S.N. Timasheff, The stabilization of proteins by osmolytes, Biophys. J. 47 (3) (1985) 411–414.
[18] C.Y. Hu, G.C. Lynch, H. Kokubo, B.M. Pettitt, Trimethylamine N-oxide influence on the backbone of proteins: an oligoglycine model, Proteins 78 (3) (2010) 695–704.
[19] D.L. Pincus, C. Hyeon, D. Thirumalai, Effects of trimethylamine N-oxide (TMAO) and crowding agents on the stability of RNA hairpins, J. Am. Chem. Soc. 130 (23) (2008) 7364–7372.
[20] M.A. Schroer, Y. Zhai, D.C.F. Wieland, C.J. Sahle, J. Nase, M. Paulus, M. Tolan, R. Winter, Exploring the piezophilic behavior of natural cosolvent mixtures, Angewandte Chem. Int. 50 (48) (2011) 11413–11416.
[21] K. Julius, J. Weine, M. Berghaus, N. König, M. Gao, J. Latarius, M. Paulus, M.A. Schroer, M. Tolan, R. Winter, Water-mediated protein-protein interactions at high pressures are controlled by a deep-sea osmolyte, Phys. Rev. Lett. 121 (2018) (S. 038101).
[22] R. Kumar, J.M. Serrett, E.B. Thompson, Osmolyte-induced folding enhances tryptic enzyme activity, Arch. Biochem. Biophys. 426 (1) (2005) 78–82.
[23] S.S. Cho, G. Reddy, J.E. Straub, D. Thirumalai, Entropic stabilization of proteins by TMAO, J. Phys. Chem. B 115 (45) (2011) 13401–13407.
[24] S. Imoto, H. Forbert, D. Marx, Water structure and solvation of osmolytes at high hydrostatic pressure: pure water and TMAO solutions at 10 kbar versus 1 bar, Phys. Chem. Chem. Phys. 17 (37) (2015) 24224–24237.
[25] C. Hölzl, P. Kibies, S. Imoto, R. Frach, S. Suladze, R. Winter, D. Marx, D. Horinek, S.M. Kast, Design principles for high-pressure force fields: aqueous TMAO solutions from ambient to kilobar pressures, J. Chem. Phys. 144 (2016) (S. 144104).
[26] S. Shimizu, P.E. Smith, How osmolytes counteract pressure denaturation on a molecular scale, ChemPhysChem 18 (2017) 2243–2249.
[27] P. Schienbein, G. Schwaab, H. Forbert, M. Havenith, D. Marx, Correlations in the solute–solvent dynamics reach beyond the first hydration shell of ions, J. Phys. Chem. Lett. 8 (2017) 2373–2380.
[28] L. Knake, H. Vondracek, M. Havenith, A novel set-up to investigate the low-frequency spectra of aqueous solutions at high hydrostatic pressure, Rev. Sci. Instrum. 87 (2016) 104101.
[29] H.B. Bohidar, Light-scattering study of solution properties of bovine serum-albumin, insulin, and polystyrene under moderate pressure, Colloid Polym. Sci. 267 (4) (1989) 292–300.
[30] C. Ma, X. Wu, F. Huang, Q. Zhou, F. Li, Q. Cui, The acoustic velocity, refractive index, and equation of state of liquid ammonia dihydrate under high pressure and high temperature, J. Chem. Phys. 137 (10) (2012).
[31] S. Vance, J.M. Brown, Thermodynamic properties of aqueous MgSO4 to 800 MPa at temperatures from- 20 to 100 degrees C and concentrations to 2.5 Mol kg(−1) from sound speeds, with applications to icy world oceans, Geochim. Cosmochim. Acta 110 (2013) 176–189.
[32] T.C. Ransom, M. Ahart, R.J. Hemley, C.M. Roland, Acoustic properties and density of polyurea at pressure up to 13.5 GPa through Brillouin scattering spectroscopy, J.

Appl. Phys. 123 (19) (2018).
[33] S. Petitgirard, W.J. Malfait, R. Sinmyo, I. Kupenko, L. Hennet, D. Harries, T. Dane, M. Burghammer, D.C. Rubie, Fate of MgSiO3 melts at core-mantle boundary conditions, Proc. Natl. Acad. Sci. U. S. A. 112 (46) (2015) 14186–14190.
[34] S. Petitgirard, W.J. Malfait, B. Journaux, I.E. Collings, E.S. Jennings, I. Blanchard, I. Kantor, A. Kurnosov, M. Cotte, T. Dane, M. Burghammer, D.C. Rubie, SiO2 glass density to lower-mantle pressures, Phys. Rev. Lett. 119 (21) (2017).
[35] H. Teng, A. Yamasaki, M.K. Chun, H. Lee, Solubility of liquid CO2 in water at temperatures from 278 K to 293 K and pressures from 6.44 MPa to 29.49 MPa and densities of the corresponding aqueous solutions, J. Chem. Thermodyn. 29 (11) (1997) 1301–1310.
[36] Z.W. Li, M.Z. Dong, S.L. Li, L.M. Dai, Densities and solubilities for binary systems of carbon dioxide + water and carbon dioxide + brine at 59 °C and pressures to 29 MPa, J. Chem. Eng. Data 49 (4) (2004) 1026–1031.
[37] E.L. Shock, H.C. Helgeson, Calculation of the thermodynamic and transport properties of aqueous species at high pressures and temperatures: correlation algorithms for ionic species and equation of state predictions to 5 kb and 1000°C, Geochim. Cosmochim. Acta 52 (8) (1988) 2009–2036.
[38] E.L. Shock, H.C. Helgeson, D.A. Sverjensky, Calculation of the thermodynamic and transport properties of aqueous species at high pressures and temperatures: standard partial molal properties of inorganic neutral species, Geochim. Cosmochim. Acta 53 (9) (1989) 2157–2183.
[39] L.M.C. Pereira, A. Chapoy, R. Burgass, B. Tohidi, Measurement and modelling of high pressure density and interfacial tension of (gas + n -alkane) binary mixtures, J. Chem. Thermodyn. 97 (2016) 55–69.
[40] K. Liu, Y. Wu, M.A. McHugh, H. Baled, R.M. Enick, B.D. Morreale, Equation of state modeling of high-pressure, high-temperature hydrocarbon density data, J. Supercrit. Fluids 55 (2) (2010) 701–711.
[41] J. Gross, G. Sadowski, Perturbed-chain SAFT: an equation of state based on a perturbation theory for chain molecules, Ind. Eng. Chem. Res. 40 (4) (2001) 1244–1260.
[42] Florian J. Wirkert, Michael Paulus, Julia Nase, Johannes Möller, Simon Kujawski, Christian Sternemann, Metin Tolan, X-ray reflectivity measurements of liquid/solid interfaces under high hydrostatic pressure conditions, J. Synchrotron Radiat. 21 (1) (2014) 76–81.
[43] D. Lützenkirchen-Hecht, R. Wagner, U. Haake, A. Watenphul, R. Frahm, The materials science X-ray beamline BL8 at the DELTA storage ring, J. Synchrotron Radiat. 16 (2009) 264–272.
[44] https://webbook.nist.gov/chemistry/fluid/.
[45] https://physics.nist.gov/PhysRefData/Xcom/html/xcom1.html.
[46] P.S.Z. Rogers, K.S. Pitzer, Volumetric properties of aqueous sodium chloride solutions, J. Phys. Chem. Ref. Data 11 (1) (1982) 15–81.
[47] D.M. Makarov, G.I. Egorov, A.M. Kolker, Density and volumetric properties of aqueous solutions of trimethylamine N-oxide in the temperature range from (278.15 to 323.15) K and at pressures up to 100 MPa, J. Chem. Eng. Data 60 (5) (2015) 1291–1299.
[48] J. Abascal, C. Vega, A general purpose model for the condensed phases of water: TIP4P/2005, J. Chem. Phys. 123 (2005) (S. 234505).
[49] John G. Kirkwood, Frank P. Buff, The statistical mechanical theory of solutions. I, J. Chem. Phys. 19 (1951) 774.
[50] R. Cortes-Huerto, K. Kremer, R. Potestio, Communication: Kirkwood-Buff integrals in the thermodynamic limit from small-sized molecular dynamics simulations, J. Chem. Phys. 145 (2016) (S. 141103).
[51] L.F. Cameretti, G. Sadowski, Modeling of aqueous amino acid and polypeptide solutions with PC-SAFT, Chem. Eng. Process. Process Intensif. 47 (6) (2008) 1018–1025.
[52] A.P. Carneiro, O. Rodriguez, C. Held, G. Sadowski, E.A. Macedo, Density of mixtures containing sugars and ionic liquids: experimental data and PC-SAFT modeling, J. Chem. Eng. Data 59 (10) (2014) 2942–2954.
[53] C. Held, G. Sadowski, Compatible solutes: thermodynamic properties relevant for effective protection against osmotic stress, Fluid Phase Equilib. 407 (2016) 224–235.
[54] M. Kleiner, G. Sadowski, Modeling of polar systems using PCP-SAFT: an approach to account for induced-association interactions, J. Phys. Chem. C 111 (43) (2007) 15544–15553.
[55] N. von Solms, M.L. Michelsen, C.P. Passos, S.O. Derawi, G.M. Kontogeorgis, Investigating models for associating fluids using spectroscopy, Ind. Eng. Chem. Res. 45 (15) (2006) 5368–5374.
[56] J. Gross, G. Sadowski, Application of the perturbed-chain SAFT equation of state to associating systems, Ind. Eng. Chem. Res. 41 (22) (2002) 5510–5515.
[57] L.F. Cameretti, G. Sadowski, J.M. Mollerup, Modeling of aqueous electrolyte solutions with perturbed-chain statistical associated fluid theory, Ind. Eng. Chem. Res. 44 (9) (2005) 3355–3362.
[58] M. Kleiner, Thermodynamic modeling of complex systems: polar and associating fluids and mixtures, Verlag Dr. Hut, (2008) PhD Thesis, TU Dortmund.
[59] K. Kiesow, F. Tumakaka, G. Sadowski, Experimental investigation and prediction of oiling out during crystallization process, J. Cryst. 310 (18) (2008) 4163–4168.
[60] W. Wagner, A. Pruß, The IAPWS formulation 1995 for the thermodynamic properties of ordinary water substance for general and scientific use, J. Phys. Chem. Ref. Data 31 (2) (2002) 387–535.
[61] C.J. Sahle, M.A. Schroer, I. Juurinen, J. Niskanen, Influence of TMAO and urea on the structure of water studied by inelastic X-ray scattering, Phys. Chem. Chem. Phys. 18 (24) (2016) 16518–16526.
[62] F. Lehmkuehler, Y. Forov, M. Elbers, I. Steinke, C.J. Sahle, C. Weis, N. Tsuji, M. Itou, Y. Sakurai, A. Poulain, C. Sternemann, Temperature dependence of the hydrogen bond network in trimethylamine N-oxide and guanidine hydrochloride-water solutions, Phys. Chem. Chem. Phys. 19 (41) (2017) 28470–28475.
[63] J. Baz, J. Gebhardt, H. Kraus, D. Markthaler, N. Hansen, Insights into noncovalent binding obtained from molecular dynamics simulations, Chem. Ingenieur Technik 90 (2018) 1864–1875.